BMSC-derived exosome-mediated miR-25-3p delivery protects against myocardial ischemia/reperfusion injury by constraining M1-like macrophage polarization

JINGXIA DU, YIBO DONG, JINGJING SONG, HANQI SHUI, CHENGYAO XIAO, YUE HU, SHIYAO ZHOU and SHANSHAN WANG

College of Basic Medicine and Forensic Medicine, Henan University of Science and Technology, Luoyang, Henan 471023, P.R. China

Received February 20, 2024; Accepted May 16, 2024

DOI: 10.3892/mmr.2024.13266

Abstract. Myocardial ischemia/reperfusion injury (MIRI) is a significant challenge in the management of myocardial ischemic disease. Extensive evidence suggests that the macrophage-mediated inflammatory response may play a vital role in MIRI. Mesenchymal stem cells and, in particular, exosomes derived from these cells, may be key mediators of myocardial injury and repair. However, whether exosomes protect the heart by regulating the polarization of macrophages and the exact mechanisms involved are poorly understood. The present study aimed to determine whether exosomes secreted by bone marrow mesenchymal stem cells (BMSC-Exo) harboring miR-25-3p can alter the phenotype of macrophages by affecting the JAK2/STAT3 signaling pathway, which reduces the inflammatory response and protects against MIRI. An *in vivo* MIRI model was established in rats by ligating the anterior descending region of the left coronary artery for 30 min followed by reperfusion for 120 min, and BMSC-Exo carrying miR-25-3p (BMSC-Exo-25-3p) were administered through tail vein injection. A hypoxia-reoxygenation model of H9C2 cells was established, and the cells were cocultured with BMSC-Exo-25-3p *in vitro*. The results of the present study demonstrated that BMSC-Exo or BMSC-Exo-25-3p could be taken up by cardiomyocytes *in vivo* and H9C2 cells *in vitro*. BMSC-Exo-25-3p demonstrated powerful cardioprotective effects by decreasing the cardiac infarct size, reducing the incidence of malignant arrhythmias and attenuating myocardial enzyme activity, as indicated by lactate dehydrogenase and creatine kinase levels. It induced M1-like macrophage polarization after myocardial ischemia/reperfusion (I/R), as evidenced by the increase in iNOS expression through immunofluorescence staining and upregulation of proinflammatory cytokines through RT-qPCR, such as interleukin-1β (IL-1β) and interleukin-6 (IL-6). As hypothesized, BMSC-Exo-25-3p inhibited M1-like macrophage polarization and proinflammatory cytokine expression while promoting M2-like macrophage polarization. Mechanistically, the JAK2/STAT3 signaling pathway was activated after I/R *in vivo* and in LPS-stimulated macrophages *in vitro*, and BMSC-Exo-25-3p pretreatment inhibited this activation. The results of the present study indicate that the attenuation of MIRI by BMSC-Exo-25-3p may be related to JAK2/STAT3 signaling pathway inactivation and subsequent inhibition of M1-like macrophage polarization.

Introduction

Acute myocardial infarction is a form of myocardial necrosis resulting from acute and persistent ischemia and hypoxia in the coronary artery and is a significant contributor to global mortality and disability rates (1-3). Effective treatment protocols involve restoring the blood supply to the ischemic myocardium as soon as possible through thrombolysis and percutaneous coronary intervention (4). However, reperfusion can further damage the ischemic myocardium, referred to as myocardial ischemia/reperfusion injury (MIRI) (5), which can affect the prognosis of patients. Currently, the main clinical treatment for myocardial ischemia is percutaneous artery intervention (PCI), however, this treatment only provides short-term relief and also leads to myocardial re-damage (6). Other current treatments, such as calcium channel blockers or hypoxia preconditioning, are used for MIRI but are not very effective, as multiple factors are involved in the pathophysiological process of MIRI (7,8), there is an urgent requirement to find more therapeutic solutions for MIRI. MIRI encompasses a range of pathophysiological mechanisms, including calcium and proton overload, endoplasmic reticulum stress, excessive oxidative stress, mitochondrial morphology and dysfunction, and activation of apoptotic pathways, ultimately leading to an inflammatory cascade within cardiac tissue (9). This inflammatory response is intricately linked to myocardial injury and the formation of scar tissue. Consequently, mitigating the

Correspondence to: Dr Jingxia Du, College of Basic Medicine and Forensic Medicine, Henan University of Science and Technology, 263 Kaiyuan Avenue, Luoyang, Henan 471023, P.R. China
E-mail: dujingxia2005@163.com

Key words: ischemia/reperfusion, exosome, miR-25-3p, macrophage polarization, JAK2, STAT3

inflammatory response is considered important in prevention and treatment strategies for MIRI (10).

Macrophages are a heterogeneous group of immune cells important for regulating inflammation and immune balance (11). Additionally, macrophages play an important role in regulating cardiac inflammation (12). The wide range of macrophage functions arises from their diversity and adaptability; macrophages detect inflammation in the heart and adjust their characteristics accordingly (13). Dependent on the microenvironment, macrophages can polarize toward the M1 or M2 phenotype. An imbalance of the M1/M2 macrophage phenotype is a known pathological marker of various inflammatory diseases (14,15), including diabetic nephropathy and atherosclerosis. Upregulated proinflammatory factor and inflammatory mediator expression is observed with the propensity macrophage M1 polarization, and preventing the polarization of M1-type macrophages within a specific immune environment is vital for regulating infections and maintaining homeostasis (16). The balance between M1- and M2-like macrophages is a potential target for treating MIRI (17).

Increasing evidence suggests that the Janus tyrosine kinase 2 (JAK2)/signal transducer and activator of the transcription 3 (STAT3) pathway regulates inflammation-related disorders, such as allergies and cardiovascular disease (18,19), and this pathway may participate in MIRI (20). Phosphorylation of JAK2 activates STAT3, the principal effector in the initiation and progression of cardiac injury (21). Following translocation from the cytoplasm to the nucleus, phosphorylated STAT3 enhances the transcription of pro-inflammatory factors (22). Activated JAK2/STAT3 signaling can promote the proliferation of RAW264.7 cells stimulated by LPS and increase the secretion of inflammation-related factors (23). This evidence suggests that inhibiting the JAK2/STAT3 signaling pathway may promote the transformation of macrophages from the M1 to the M2 phenotype; thus, this pathway may play a key role in the treatment of MIRI.

Mesenchymal stem cells (MSCs) are a unique type of stromal cell with the potential to differentiate into multiple cell types and the ability to regulate the phenotype and function of immune cells (24). The use of MSCs are considered a potential new strategy for treating autoimmune and inflammatory diseases and have functional and structural benefits in treating ischemic heart disease (25). The transplantation of bone marrow MSCs (BMSCs) has been explored as a potential treatment for repairing ischemic heart injuries, whereby BMSCs transplanted into the ischemic heart can differentiate into endothelial, vascular smooth muscle and myocardial-like cells (26). Nevertheless, the low cell survival rate and potential biosafety issue reduce the effectiveness of cell therapy (27,28).

Exosomes, the smallest extracellular vesicles with a typical diameter of 50-150 nm, are released by various cell types and have multiple beneficial effects such as exerted obvious cardioprotection by increasing cardiac function and limiting pathological remodeling, including cardiac hypertrophy and cardiac fibrosis (29). Using exosomes secreted by BMSCs (BMSC-Exo) instead of BMSCs to treat MIRI is a potentially beneficial cell-free treatment strategy (30). BMSC-Exo accounts for a large portion of circulating microvesicles (31). Although numerous studies have shown that BMSC-Exo can alleviate MIRI (32,33), at present, the understanding of BMSCs and BMSC-Exo is still in the infancy stage. For example, the outcome *in vivo* is unknown, the long-term implantation consequences are uncertain and the underlying mechanisms require further exploration. Notably, exosome-mediated cell-to-cell interactions involve various miRNAs that play significant roles in inflammation, tissue repair and fibrogenesis (34). For example, miR-494 is cardioprotective in MIRI by targeting apoptosis-related proteins (35), miR-148a alleviates hepatic ischemia/reperfusion (I/R) injury by improving liver function and suppressing hepatocellular apoptosis (36), and overexpression of BMSC-Exo-125b can enhance the viability of myocardial cells after MIRI and inhibit cell apoptosis (37). Moreover, extracellular vesicles derived from MSCs can exert important protective effects on the heart by overexpressing miR-25-3p, promoting myocardial cell survival and inhibiting inflammation *in vivo* and *in vitro (*38). However, few studies have investigated the exact mechanism through which BMSC-Exo-25-3p protects against inflammation during MIRI.

In the present study the therapeutic potential of BMSC-Exo-25-3p against MIRI was explored and the underlying mechanism was investigated by establishing an *in vivo* MIRI model and an *in vitro* hypoxia-reoxygenation (H/R) cell model. The present study provides a potential therapeutic approach for MIRI, with the aim to provide new therapeutic drugs and approaches to improve the prognosis of patients with coronary heart disease after thrombolysis or percutaneous coronary intervention.

Materials and methods

Experimental animals. A total of 40 Sprague-Dawley (SD) male rats (age, 8-week-old; weight, 200±20 g) were obtained from The Experimental Animal Center of Tongji Medical College, Huazhong University of Science and Technology (Wuhan, China; license no. SCXK 2019-0002). The animals were housed in a controlled environment with a 12-h light/dark cycle, at 22±2˚C and 50±5% humidity, with free access to food and water. All the experimental procedures were approved by The Animal Care and Ethics Committee of Henan University of Science and Technology (Luoyang, China; approval no. 2021-0392).

Extraction of primary BMSCs. In the present study, 20 male rats (age, 3-week-old; weight, 50±5 g) were obtained from The Experimental Animal Center of Tongji Medical College, Huazhong University of Science and Technology (Wuhan, China; license no. SCXK 2018-0005). The animals were housed in a controlled environment with a 12-h light/dark cycle, at 22±2˚C and 50±5% humidity, with free access to food and water. The rats were euthanized by cervical dislocation and immersed in 75% alcohol for 10 min. The front and back legs were stripped, and the bone marrow cavity was cleaned by adding serum-free culture solution via a syringe. The cell suspension was passed through a 75-μm cell strainer to eliminate any tissue, fat or debris. Subsequently, the mixture was centrifuged at 300 x g for 5 min at room temperature, and the resulting pellet was resuspended in ACK lysis buffer (Beijing Solarbio Science & Technology Co., Ltd.) at room temperature for 2 min. The cells were washed with minimum essential medium α (MEM; Wuhan Pricella Biotechnology

Co., Ltd.) supplemented with 10% fetal bovine serum (FBS; Beijing Solarbio Science & Technology Co., Ltd.) and centrifuged at 300 x g for 5 min at room temperature. After which, the cells were collected and cultured in MEM supplemented with 10% FBS at 37˚C with 5% CO_2. After 48 h of culture, the half-volume exchange method was used whereby half of the original medium was replaced with an equal amount of fresh medium. Subsequently, the medium was changed every 3 days until the cells reached 90% confluence at 37˚C, at which point primary BMSCs could be obtained (39).

Extraction and identification of BMSC-Exo. The culture supernatant of the BMSCs was collected when the cell density reached 80-90%. The cell supernatant was centrifuged at 2,000 x g at 4˚C for 10 min to remove the nonadherent cells. After which, the supernatant was collected and centrifuged at 10,000 x g at 4˚C for 30 min to remove cell fragments. The supernatant was subsequently centrifuged at 100,000 x g for 90 min at 4˚C in an ultracentrifuge (Sorvall™ WX+; Thermo Fisher Scientific, Inc.). The supernatant was carefully removed, and an appropriate volume of PBS was added to resuspend the pellet containing the BMSC-Exo. The BMSC-Exo was filtered (0.22-μm) and stored at -80˚C for subsequent detection and use. A total of 20 ul of the resuspended samples were added dropwise to 200-mesh copper grids. Tissue sections (0.1-μm thick) were incubated at room temperature for 10 min, fixed in 3% glutaraldehyde at 4˚C for 2 h. After which, the grids were negatively stained with 2% phosphotungstic acid (Shanghai Macklin Biochemical Co., Ltd.) at room temperature for 3 min, and the remaining liquid was removed by filter paper. BMSC-Exo morphology was assessed via transmission electron microscopy (TEM; JEM1400; JEOL, Ltd.; Digital Micrograph 3.5, Gatan, Inc.) at an accelerating voltage of 80 kV. BMSC-Exo nanoparticle tracking analysis (NTA) was performed with a Zetasizer Nano (Malvern Instruments, Ltd.), and BMSC-Exo biomarkers were detected by western blotting.

Loading of BMSC-Exo with miR-25-3p by electroporation. A total of 500 μl BMSC-Exo (250 μM) and 100 μg of miR-25-3p (Shanghai GenePharma Co., Ltd.) were gently mixed in 400 μl cold electroporation buffer (MEM-α reduced serum medium; 1.15 mM K3PO4 pH 7.2 and 25 mM KCl, conductivity and osmolarity were 300 mOsm/kg, 10 ms/cm) and incubated for 5 min at room temperature, as previously described (40). Electroporation was performed in a 4-mm cuvette using a 0.35-sec pulse repeated 20 times at 0.7 kV and 50 μF (the electrode material was a conductive polymer with a diameter range of 0.3 mm, the time interval between each pulse was 20 sec and the repetition frequency was 300 Hz) by an electroporation instrument (SCIENTZ-2C; Ningbo Scientz Biotechnology, Co., Ltd.) as previously described (40). After which, the mixture was incubated with MEM-α for 30 min at 4˚C to recover the membrane structure, and washed twice with ice-cold PBS buffer by ultracentrifugation at 10^5 x g for 70 min at 4˚C to remove free miRNAs. The pellet was then resuspended in PBS and stored at -80˚C for subsequent use, and it was ensured that reagents were used within 1 week.

Evaluating BMSC-Exo internalization in vivo and in vitro. BMSC-Exo and DiR dye (Shanghai Aladdin Biochemical Technology Co., Ltd.) were incubated at 37˚C for 30 min and then subjected to ultracentrifugation for 1 h at 100,000 x g at room temperature to remove the remaining dye. Subsequently, rats were injected with DiR-BMSC-Exo (1 ml; 100 μg/kg) through the tail vein, and the BMSC-Exo organ distribution was dynamically observed within 24 h using a small animal imaging device (FUSION FX EDGE SPECTRA; Vilber Lourmat) (41). Similarly, H9C2 cells (The Cell Bank of Type Culture Collection of The Chinese Academy of Sciences) were cocultured with Dil-labeled BMSC-Exo for 6 h at 37˚C and then fixed in 4% paraformaldehyde for 20 min at 25˚C. BMSC-Exo internalization by H9C2 cells was evaluated via confocal microscopy (Nikon Corporation) (42).

Establishment of in vivo MIRI models and animal grouping. As previously described (43), 40 rats were randomly divided into 4 groups: i) Sham; ii) I/R + PBS; iii) I/R + BMSC-Exo; and iv) I/R + BMSC-Exo-25-3p (n=10/group). BMSC-Exo or BMSC-Exo-25-3p (100 μg/kg) were injected through the tail vein 2 h before I/R surgery. The rats were deeply anesthetized with pentobarbital sodium (50 mg/kg, i.p.) and fixed on the operating table. Occasionally, 1/4 of the initial dose was added when needed during the experiment by observing the responses of that rats, such as muscle tension and response to skin pinch. A ventilator was attached to keep the animal mechanically ventilated. Electrocardiograms were recorded continuously during the experiment using the HF-12 movable functional experimental platform (Chengdu Taimeng Software Co., Ltd.). The chest cavity was opened at the fourth intercostal space, exposing the heart. An *in vivo* MIRI model was established in rats by ligating the anterior descending coronary artery for 30 min followed by reperfusion for 120 min. In the sham group, the left anterior descending of coronary artery was threaded without ligation.

Triphenyl tetrazolium chloride (TTC) staining for myocardial infarction size measurement. At the end of the experiment, all rats were immediately euthanized by rapid injection of pentobarbital sodium (150 mg/kg, i.p.). The hearts were immediately removed and rinsed with saline to remove residual blood, and the remaining saline was removed with filter paper. The hearts were frozen at -80˚C for 5 min, cut into small slices, immersed in 1% TTC (BIOSS) for 20 min at 37˚C and images were captured. The area of the noninfarct (indicated in red) and infarct (shown in white) regions were determined using Image-Pro analysis software (version 6.0; Media Cybernetics, Inc.). The infarct area was calculated using the following formula: Myocardial infarct area (%)=myocardial infarct area/total myocardial area x100%.

Immunofluorescence staining. Left ventricular samples were fixed in 4% paraformaldehyde at room temperature for 24 h and then embedded in paraffin for subsequent morphological analysis. Sections (4-5-μm thick) were obtained from paraffin-embedded samples, and then deparaffinized using dimethylbenzene for 10 min, followed by rehydration in descending alcohol series for 15 min at room temperature, blocked with 3% BSA for 30 min at room temperature.

Subsequently, the sections were incubated with an anti-CD163 antibody (1:200; CST Biological Reagents Co., Ltd.) and anti-inducible nitric oxide synthase (iNOS) antibody (1:300; CST Biological Reagents Co., Ltd.) at 4˚C overnight. Following three 10-min washes with PBS, the samples were incubated with the fluorescent-labeled secondary antibodies (1:300; cat. no. GB21303; Wuhan Servicebio Technology Co., Ltd.) in the dark for 1 h at room temperature. After counter-staining with 1 μg/ml DAPI for 5 min at room temperature, the sections were viewed under a fluorescence microscope (Nikon Corporation).

Establishment of the H/R model in H9C2 cells. The H/R model was established as previously described (44). H9C2 cells were subjected to H/R *in vitro* to establish the MIRI model. Specifically, hypoxia was induced using a hypoxic incubator containing 95% nitrogen (N_2) and 5% carbon dioxide (CO_2). The culture medium (90% DMEM + 10% FBS) was replaced with serum-free medium, specifically, 100% DMEM, and the cells were incubated for 12 h in an incubator with 95% N_2 and 5% CO_2 at 37˚C. After which, the serum-free medium was replaced with a normal medium (90% DMEM + 10% FBS), and the cells were incubated for 12 h under reoxygenation conditions in an environment containing 95% air and 5% CO_2 at 37˚C (45). The grouping of the cell experiments was similar to that of the animal experiments: i) Control; ii) H/R + PBS; iii) H/R + BMSC-Exo; and iv) H/R + BMSC-Exo-25-3p. The control group was kept in a normal culture environment without H/R treatment.

Culture of macrophages and preparation of conditioned medium (CM). RAW 264.7 macrophages (The Cell Bank of Type Culture Collection of The Chinese Academy of Sciences) were used to obtain a CM for the *in vitro* experiments. RAW 264.7 macrophages were cultured in Roswell Park Memorial Institute 1640 medium (Beijing Solarbio Science & Technology Co., Ltd.) supplemented with 10% FBS at 37˚C in a humidified atmosphere containing 5% CO_2. After seeding into 25 cm^2 dishes, the RAW 264.7 macrophages were assigned to the control, LPS + PBS, LPS + BMSC-Exo and LPS + BMSC-Exo-25-3p groups. Macrophages in the control group were left untreated. In the LPS + PBS treatment, 1 μg/ml LPS (Beijing Solarbio Science & Technology Co., Ltd.) was added for 6 h at 37˚C to induce an inflammatory environment, after which PBS was added for 48 h. In the LPS + BMSC-Exo and LPS + BMSC-Exo-25-3p treatments, 1 μg/ml LPS was added for 6 h, after which BMSC-Exo (200 μl; 500 μg/ml) or BMSC-Exo-25-3p (200 μl; 500 μg/ml) were added for 48 h at 37˚C (46). Subsequently, the culture medium was collected and passed through a 0.22-μm filter to obtain the CM. H9C2 cells were then cultured with the CM, washed twice with PBS and collected for further molecular biological analyses. The CM includes culture supernatants from the corresponding treatments of the LPS + PBS group, the LPS + BMSC-Exo group and the LPS + BMSC-Exo-25-3p group, which were used as the conditioned media termed CM1, CM2 and CM3, respectively.

Treatment of H9C2 cells with CM. H9C2 cells were treated with CM obtained as aforementioned for 24 h at 37˚C, after which the H/R model was established as aforementioned per the experimental requirements and different processing methods. At the end of the cell treatment, the supernatant was collected to analyze the creatine kinase (CK) and lactate dehydrogenase (LDH) enzyme activity, which reflect myocardial cell damage.

Measurement of CK and LDH activity. Myocardial injury was assessed by the activity of CK and LDH in blood samples and the H9C2 cell culture supernatant. The blood samples and supernatant were centrifuged at 1,716 x g at 4˚C for 15 min, and the activity of CK (Creatine Kinase Assay Kit; cat. no. A032-1-1) and LDH (Lactate Dehydrogenase Assay Kit; cat. no. A020-2-2) were measured following the manufacturer's instructions (Nanjing Jiancheng Bioengineering Institute).

Reverse transcription quantitative-polymerase chain reaction. Total RNA from the tissue and cells was isolated using TRIzol® reagent (CoWin Biosciences) and reverse-transcribed using a high-capacity complementary DNA RT kit (CoWin Biosciences). The reaction mixture was incubated at 25˚C for 10 min, followed by 50˚C for 15 min and then 85˚C for 5 min. The sequence of collar primers for miR-25-3p reverse transcription: 5'-GTCGTATCCAGTGCAGGGTCCGAG GTATTCGCACTGGATACGACTCAGAC-3'. RT-qPCR was conducted on a 7500 Sequence Detection System (Applied Biosystems; Thermo Fisher Scientific, Inc.) using a SYBR Green PCR Master Mix Kit (CoWin Biosciences) following the manufacturer's instructions, and normalized to the internal reference gene U6. The thermocycling conditions included: Pre-denaturation at 95˚C for 10 min; and annealing at 60˚C for 1 min. The expression levels of inflammatory factors, including interleukin-6 (IL-6), iNOS, interleukin-10 (IL-10) and arginase-1 (Arg-1), were determined. The primer sequences are shown in Tables SI and SII. Relative gene expression levels were quantified using the $2^{-\Delta\Delta Cq}$ method and normalized to the internal reference genes β-actin.

Western blotting. Total proteins (from exosomes, hearts and H9C2 cells) were extracted using a lysis buffer (RIPA; Beijing Solarbio Science & Technology Co., Ltd.). The protein concentration was measured using the BCA method, and the percentage of separation gel was 10%. The 40 μg protein samples were loaded onto SDS-PAGE gels, electrophoresis for 1.5 h at room temperature, maintaining a constant voltage of 80 V (Bio-Rad Laboratories, Inc.). After electrophoresis, the proteins were transferred onto PVDF membranes (Millipore Sigma), maintaining a constant current of 300 mA for 2 h at 4˚C. The samples were subsequently blocked for 1 h at room temperature with 5% BSA in TBST (0.5% Tween) buffer. The membrane was then incubated with primary antibodies overnight in 5% BSA (Merck KGaA) at 4˚C. After being washed thrice with TBS-T, the membrane was incubated with a secondary antibody diluted at 1:5,000 for 1 h at room temperature. The signal was detected using an enhanced chemiluminescence detection system (Amersham; Cytiva). The primary antibodies used were against CD9 (1:500; cat. no. WL01236, Wanleibio Co., Ltd.), CD63 (1:1,000; cat. no. D111314-0100100; Sangon Biotech Co., Ltd.), JAK2 (1:1,000; cat. no. 3203; Cell Signaling Technology, Inc.), phosphorylated (p-)JAK2 (1:1,000; cat. no. 37745; Cell Signaling Technology, Inc.), STAT3 (1:2,000;

cat. no. 9139; Cell Signaling Technology, Inc.), p-STAT3 (1:2,000; cat. no. 9145; Cell Signaling Technology, Inc.) and GAPDH (1:5,000; cat. no. P07486; Sangon Biotech Co., Ltd.). ImageJ software (version 6; National Institutes of Health) was used to analyze the bands quantitatively.

Statistical analysis. The data are presented as the mean ± SD (whole animal experiments, n=8; molecular biology experiment and the cell experiment; n=4). All the experimental data were analyzed using one-way analysis of variance followed by Tukey's multiple comparison test by GraphPad Prism 9.0 (Dotmatics). $P<0.05$ was considered to indicate a statistically significant difference.

Results

BMSC-Exo identification. TEM, NTA and surface protein marker analysis were used as the basic criteria for BMSC-Exo identification (28). TEM revealed circular bilayer lipid vesicles in BMSC-Exo (Fig. 1A). Western blotting demonstrated that CD63 and CD9 were highly expressed in the isolated particles and weakly or not expressed in the cells (Fig. 1B). NTA also revealed that the BMSC-Exo diameter peaked at 130-150 nm (Fig. 1C). These data revealed that the particles extracted from the BMSCs were BMSC-Exo.

BMSC-Exo internalization into the heart in vivo. MiR-25-3p plays an important protective role in myocardial infarction (47,48). To determine the biological role and mechanism of exogenous miR-25-3p, an exosome delivery system was designed containing miR-25-3p via BMSC-Exo, referred to as BMSC-Exo-25-3p. The loading efficiency of miR-25-3p in exosomes was evaluated via RT-qPCR and, as shown in Fig. 1D, miR-25-3p expression increased significantly in BMSC-Exo-25-3p compared with BMSC-Exo or BMSC-Exo loaded with a miR-25-3p random sequence as a negative control. A rat model of MIRI was generated via treatment with BMSC-Exo-25-3p, and the results showed that the expression of the miR-25-3p gene in the heart decreased in the I/R model rats but increased significantly after the delivery of BMSC-Exo-25-3p (Fig. 1E). These results indicated that the heart has a high affinity for BMSC-Exo-25-3p, and cardiac delivery of miR-25-3p was successful.

In vivo imaging was performed to observe the distribution of BMSC-Exo-25-3p in rats. Imaging within 12 h after intravenous injection showed that BMSC-Exo-25-3p was ingested by multiple organs, including the heart. Following these findings, the heart was removed for imaging and the fluorescence intensity was considerable (Fig. 1F). The results showed that the heart had a high affinity for BMSC-Exo.

BMSC-Exo-25-3p alleviated MIRI in vivo. To explore whether BMSC-Exo-25-3p has a protective effect on MIRI *in vivo*, myocardial infarction size was detected by TTC staining, and the incidence of malignant arrhythmia was calculated via electrocardiogram. Moreover, myocardial enzyme activity was measured as aforementioned. As shown in Fig. 2, BMSC-Exo-25-3p exerted cardioprotective effects by decreasing the cardiac infarct size (Fig. 2A and B). The incidence of malignant arrhythmias was significantly greater in the I/R group than in the sham group and significantly lower in the BMSC-Exo-25-3p treatment group (Fig. 2C). Similarly, compared with those in the sham group, the LDH and CK levels in the serum were significantly greater after I/R, whereas BMSC-Exo-25-3p treatment reversed these trends (Fig. 2D and E).

BMSC-Exo-25-3p constrains M1-like macrophage polarization and inhibits the JAK2/STAT3 signaling pathway activation in vivo. Activated macrophages can be divided into two main subtypes: M1-like (classically activated macrophages) and M2-like (alternatively activated macrophages) (49). First, immunofluorescence staining was used to detect macrophage subtypes using different macrophage markers of iNOS (M1-like) and CD163 (M2-like). As shown in Fig. 3A and B, BMSC-Exo-25-3p constrained M1-like macrophage polarization and promoted M2-like macrophage polarization. M1-like macrophages can secrete various proinflammatory cytokines, chemokines and inflammatory mediators, such as interleukin-1β (IL-1β) and interleukin-6 (IL-6) (50), while M2-like macrophages can release anti-inflammatory factors, such as IL-10 and Arg-1. Therefore, the level of inflammatory factors can indirectly reflect differences in macrophage polarization. RT-qPCR revealed that BMSC-Exo-25-3p delivery notably decreased the mRNA expression of IL-1β and IL-6 in myocardial tissue (Fig. 3C and D). Moreover, BMSC-Exo-25-3p delivery increased the mRNA expression of IL-10 and Arg-1 in myocardial tissue (Fig. 3E and F). JAK2/STAT3 signaling pathway activation is closely related to inflammation (51). It was found that JAK2/STAT3 signaling pathway activation increased after MIRI, and BMSC-Exo-25-3p delivery reversed this effect. The aforementioned results indicated that overexpression of miR-25-3p alleviates the I/R-induced inflammatory response and inhibits the JAK2/STAT3 signaling pathway (Fig. 3G-I).

Uptake of BMSC-Exo-25-3p by H9C2 cells in vitro. H9C2 cells were cocultured with BMSC-Exo-25-3p labeled with Dil. Endocytotic BMSC-Exo generated from H9C2 cells were observed via confocal microscopy (Fig. 4A). RT-qPCR revealed that miR-25-3p expression decreased after H/R. Intracellular miR-25-3p expression increased significantly in the normal H9C2 cells and the H9C2 cells with H/R-induced injury after BMSC-Exo delivery (Fig. 4B and C), indicating that BMSC-Exo-25-3p was engulfed by H9C2 cells and that BMSC-Exo successfully delivered miR-25-3p to H9C2 cells.

BMSC-Exo-25-3p alleviated H/R-induced H9C2 cell injury. Given the *in vivo* results, enzymatic activity testing was conducted on the culture medium of H9C2 cells. It was found that, after H/R treatment, the enzymatic activity of CK and LDH increased significantly compared with that in the control group, whereas BMSC-Exo-25-3p pretreatment reversed these trends and reduced the levels of CK and LDH after H/R (Fig. 4D and E). These results indicated that miR-25-3p delivered by BMSC-Exo has a direct protective effect on H9C2 cell injury caused by H/R.

Consistent with the *in vivo* experiments, a trend toward JAK2/STAT3 signaling pathway activation after H/R treatment was observed in H9C2 cells, while this trend was

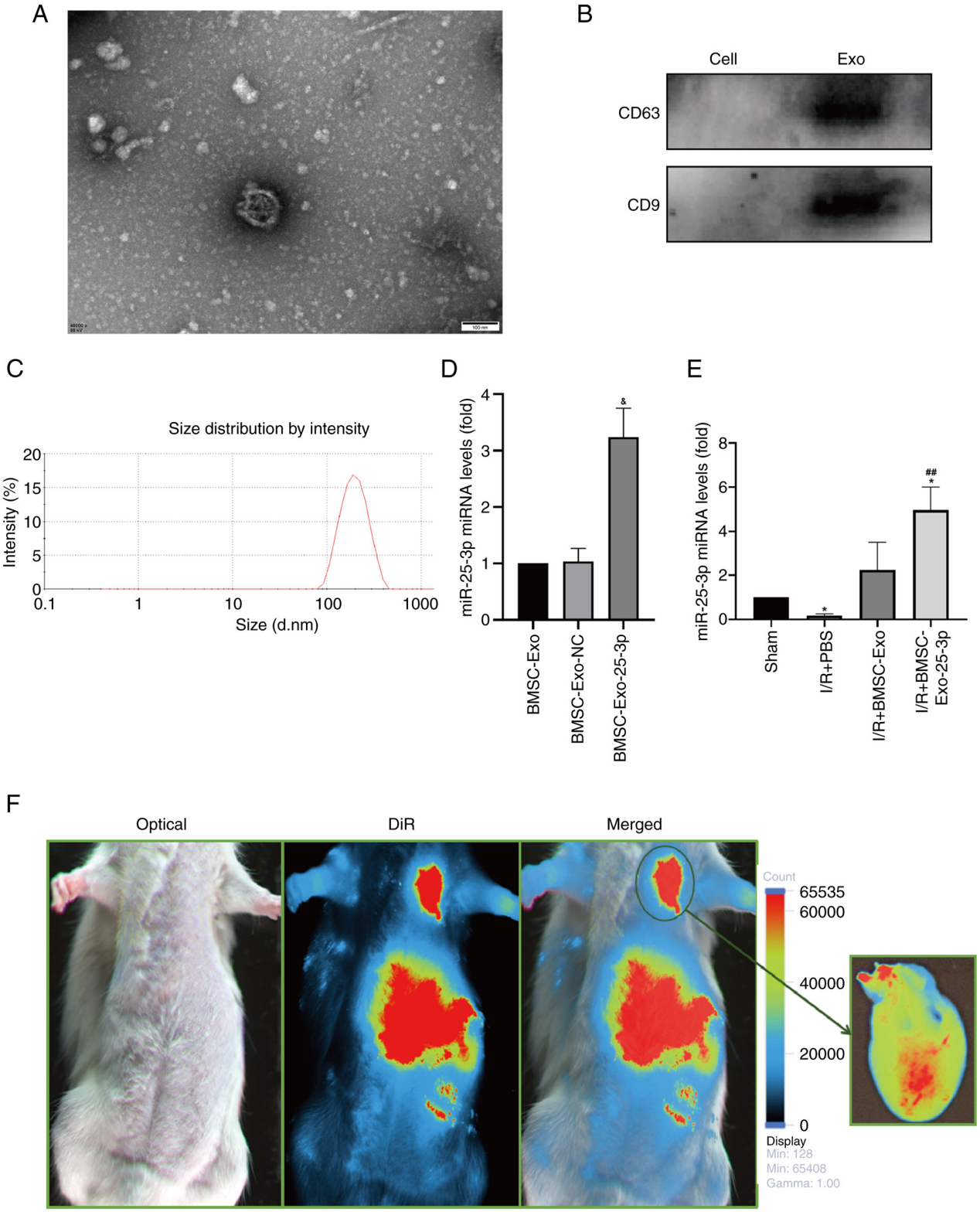

Figure 1. BMSC-Exo identification and internalization into the heart *in vivo*. (A) Representative images of BMSC-Exo by transmission electron microscope. (B) BMSC-Exo was validated by assessing exosomal protein markers. (C) Diameter distribution of BMSC-Exo was analyzed by Zetasizer Nano. (D) Expression of miR-25-3p in exosomes was assessed by RT-qPCR. (E) Expression of miR-25-3p in myocardial tissue was assessed by RT-qPCR. (F) Phagocytosis of DiR-labeled BMSC-Exo was determined by small animal imaging technology. *P<0.05 vs. sham group, $^{\#\#}$P<0.01 vs. I/R + PBS group, $^{\&}$P<0.01 vs. BMSC-Exo group or BMSC-Exo-NC group. All data were presented as mean ± SD. Exo, exosome; NC, negative control; I/R, ischemia/reperfusion; BMSC, bone marrow mesenchymal stem cells.

weakened after overexpression of miR-25-3p, suggesting that BMSC-Exo-25-3p directly inhibited the JAK2/STAT3 signaling pathway in H9C2 cells (Fig. 4F-H).

Uptake of BMSC-Exo-25-3p by RAW 264.7 macrophages in vitro. To confirm that BMSC-Exo-25-3p has an indirect protective effect on heart injury, whether the protective effect

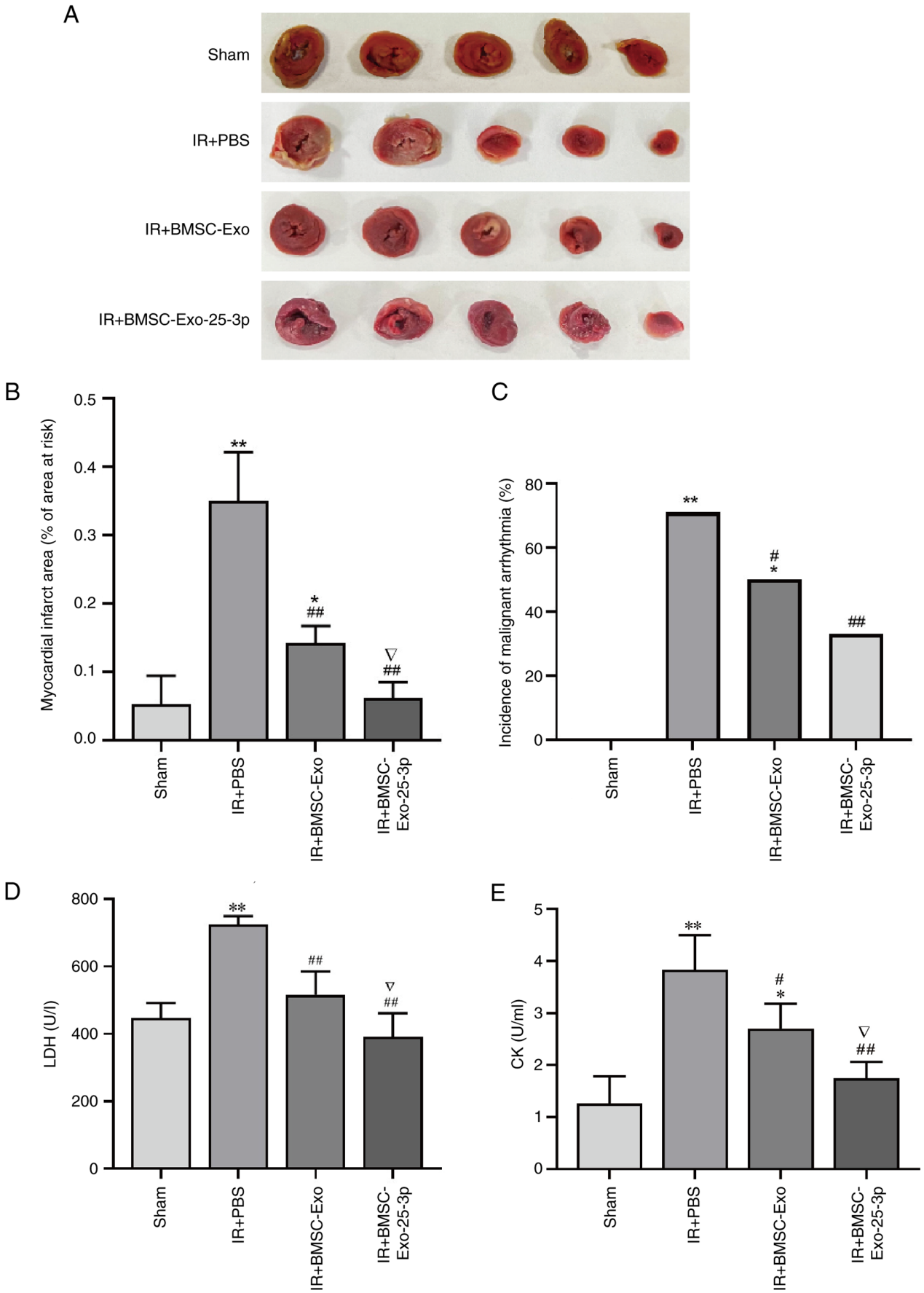

Figure 2. BMSC-Exo-25-3p alleviated MIRI in rats. (A) Representative images of the hearts sections stained with TTC. (B) Average infarct size. (C) Incidence of malignant arrhythmia by ECG. (D) LDH and (E) CK activity in serum. **P<0.01, *P<0.05 vs. sham group. $^{\#\#}$P<0.01, $^{\#}$P<0.05 vs. I/R + PBS group. $^{\nabla}$P<0.05 vs. I/R + BMSC-Exo group. All data were presented as mean ± SD. Exo, exosome; I/R, ischemia/reperfusion; BMSC, bone marrow mesenchymal stem cells; TTC, triphenyltetrazolium chloride; LDH, lactate dehydrogenase; CK, creatine kinase; MIRI, myocardial ischemia/reperfusion injury.

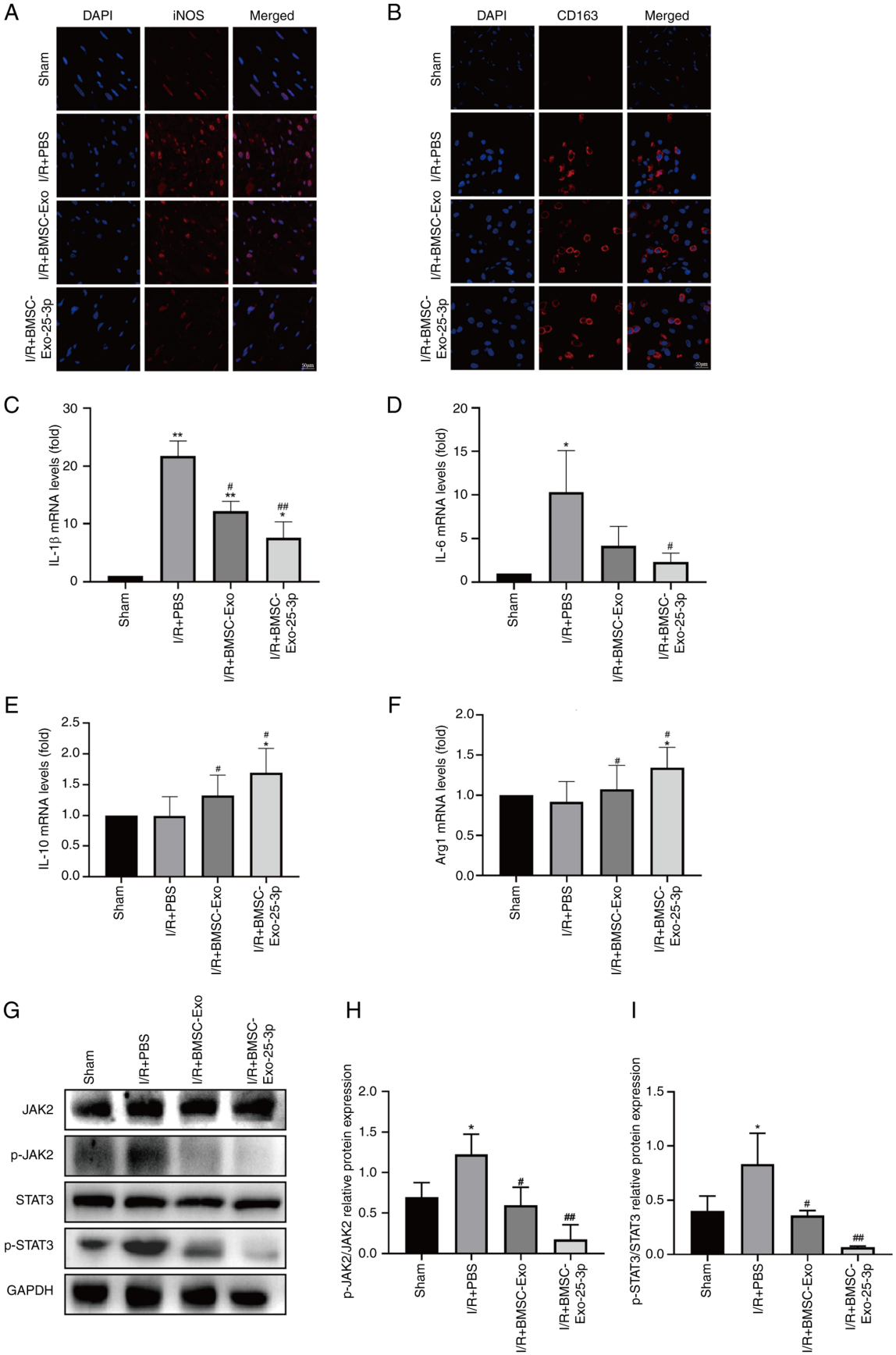

Figure 3. BMSC-Exo-25-3p inhibited I/R-induced inflammatory response in rats. Immunofluorescence staining of (A) iNOS and (B) CD163 of myocardial tissue (scale bar, 50 μm). Gene expression of proinflammatory cytokines (C) IL-1β and (D) IL-6 in myocardial tissue. Gene expression of anti-inflammatory cytokines (E) IL-10 and (F) Arg-1 in myocardial tissue. (G) Representative western blotting images of the JAK2/STAT3 signaling pathway. Quantitative analysis of (H) p-JAK2 and (I) p-STAT3. **P<0.01, *P<0.05 vs. Sham group. $^{\#\#}$P<0.01, $^{\#}$P<0.05 vs. I/R + PBS group. All data were presented as mean ± SD. Exo, exosome; I/R, ischemia/reperfusion; BMSC, bone marrow mesenchymal stem cells; IL, interleukin; Arg-1, Arginase-1; JAK2, Janus kinase 2; p-, phosphorylated; STAT3, signal transducer and activator of transcription 3.

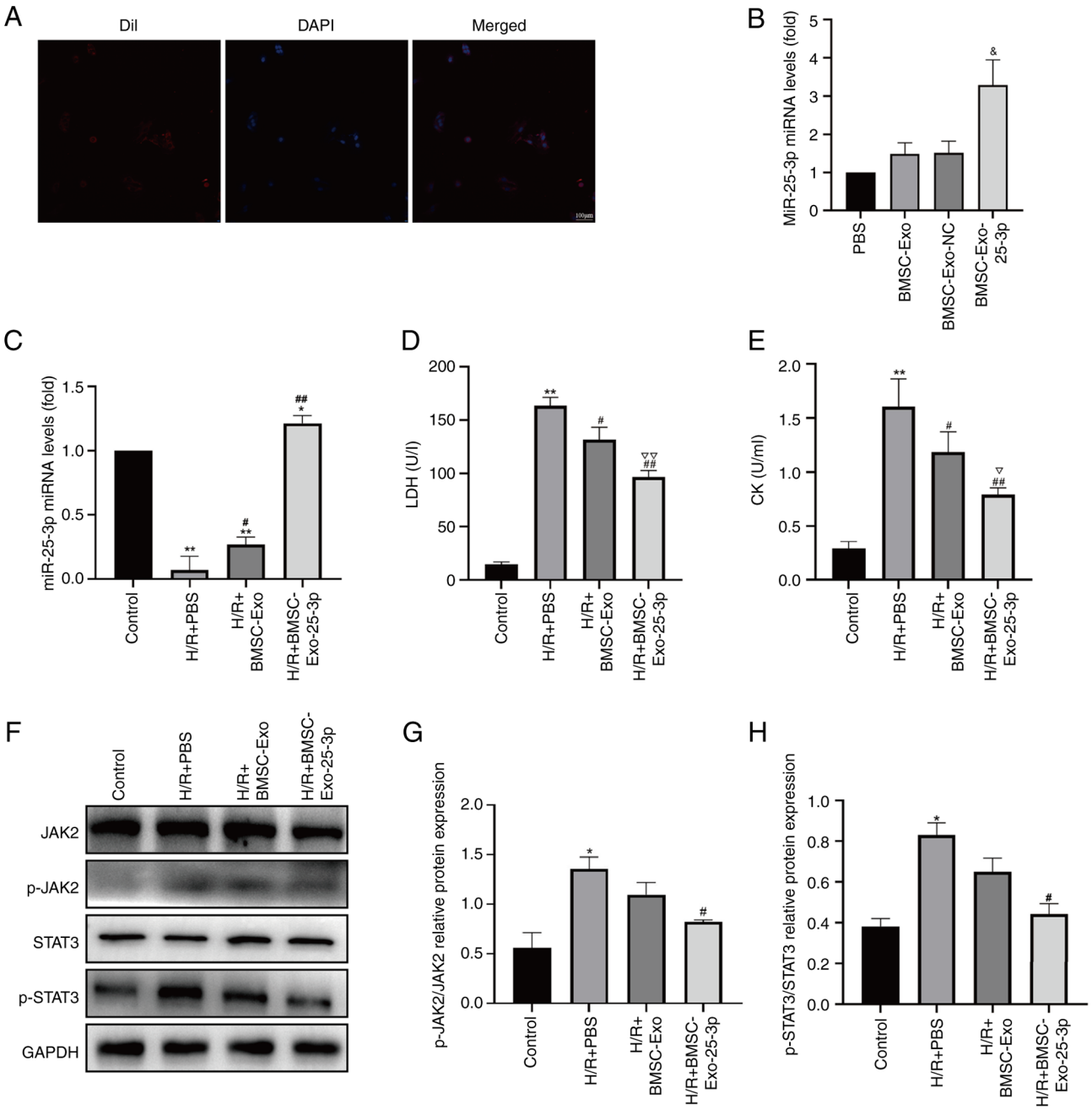

Figure 4. BMSC-Exo-25-3p alleviated H/R-induced injury in H9C2 cells. (A) Phagocytosis of Dil-labeled BMSC-Exo in H9C2 cells observed by a confocal microscope (scale bar, 50 μm). (B) Expression of miR-25-3p in H9C2 cells after co-incubation assessed by RT-qPCR. (C) Expression of miR-25-3p in H/R-induced injury in H9C2 cells. (D) LDH and (E) CK activity in cell culture supernatant. (F) Representative western blotting images of the JAK2/STAT3 signaling pathway. Quantity analysis of (G) p-JAK2 and (H) p-STAT3 in H9C2 cells. **P<0.01, *P<0.05 vs. control group. $^{\#\#}$P<0.01, $^{\#}$P<0.05 vs. H/R + PBS group. $^{\triangledown}$P<0.05 vs. H/R + BMSC-Exo group. $^{\&}$P<0.01 vs. PBS group, BMSC-Exo group or BMSC-Exo-NC group. All data were presented as mean ± SD. Exo, exosome; BMSC, bone marrow mesenchymal stem cells; NC, negative control; H/R, hypoxia/reoxygenation; LDH, lactate dehydrogenase; CK, creatine kinase; JAK2, Janus kinase 2; p-, phosphorylated; STAT3, signal transducer and activator of transcription 3.

of BMSC-Exo-25-3p on the heart was related to the regulation of macrophage polarization was examined. BMSC-Exo-25-3p labeled with Dil was cocultured with RAW 264.7 macrophages, and endocytosis by RAW 264.7 macrophages was observed via confocal microscopy (Fig. 5A).

BMSC-Exo-25-3p constrains M1-like macrophage polarization. After RAW 264.7 macrophages were stimulated with LPS, RT-qPCR was used to measure the gene expression of M1-characterizing cytokines, including IL-6 and iNOS, and M2-characterizing cytokines, including IL-10 and Arg-1. The results showed that the levels of IL-6 and iNOS in the LPS treatment group were significantly increased. However, pretreatment with BMSC-Exo-25-3p reversed these effects, reducing the expression of IL-6 and iNOS (Fig. 5B and C) and increasing the expression of IL-10 and Arg-1 significantly in RAW 264.7 macrophages after LPS stimulation (Fig. 5D and E). These results suggested that BMSC-Exo-25-3p inhibits M1-like macrophage polarization and accelerates M2-like polarization.

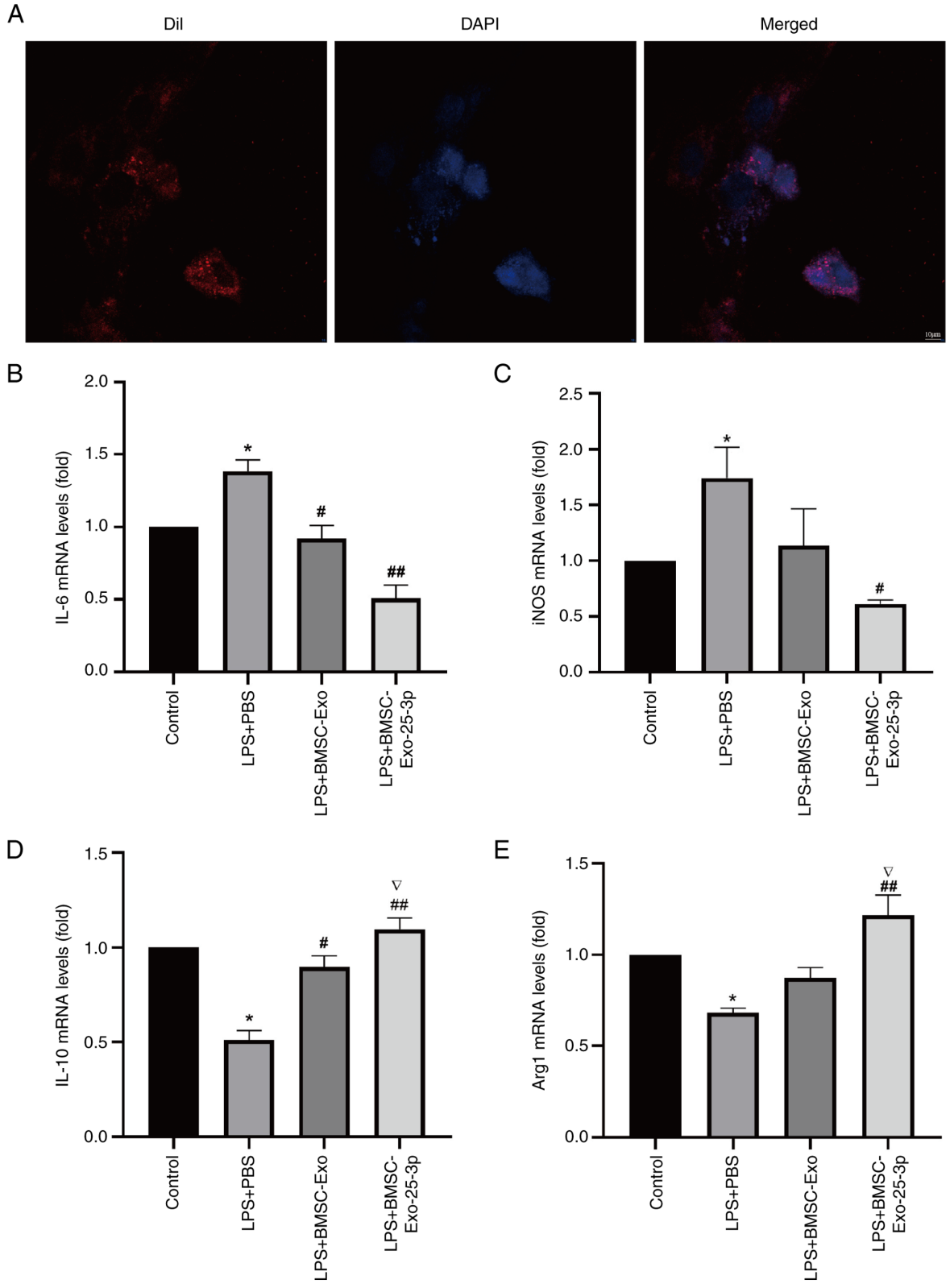

Figure 5. BMSC-Exo-25-3p constrained M1-like macrophage polarization in RAW 264.7 cells. (A) Phagocytosis of Dil-labeled BMSC-Exo in RAW 264.7 cells observed by confocal microscope, bar=10 μm. Gene expression of proinflammatory cytokines (B) IL-6 and (C) iNOS in LPS-stimulated RAW 264.7 cells. Gene expression of anti-inflammatory cytokines (D) IL-10 and (E) Arg-1 in LPS-stimulated RAW 264.7 cells. *P<0.05 vs. control group. $^{\#\#}$P<0.01, $^{\#}$P<0.05 vs. LPS + PBS group. $^{\triangledown}$P<0.05 vs. LPS + BMSC-Exo group. All data were presented as mean ± SD. Exo, exosome; BMSC, bone marrow mesenchymal stem cells; LPS, lipopolysaccharide; IL, interleukin; iNOS, inducible nitric oxide synthase; Arg-1, Arginase-1.

Mechanistically, western blotting was performed to measure the expression levels of proteins related to the JAK2/STAT3 signaling pathway, given its involvement in regulating macrophage polarization in several pathological processes including regulation of the immune response and involvement in disease recovery in the late inflammatory phase (52). The

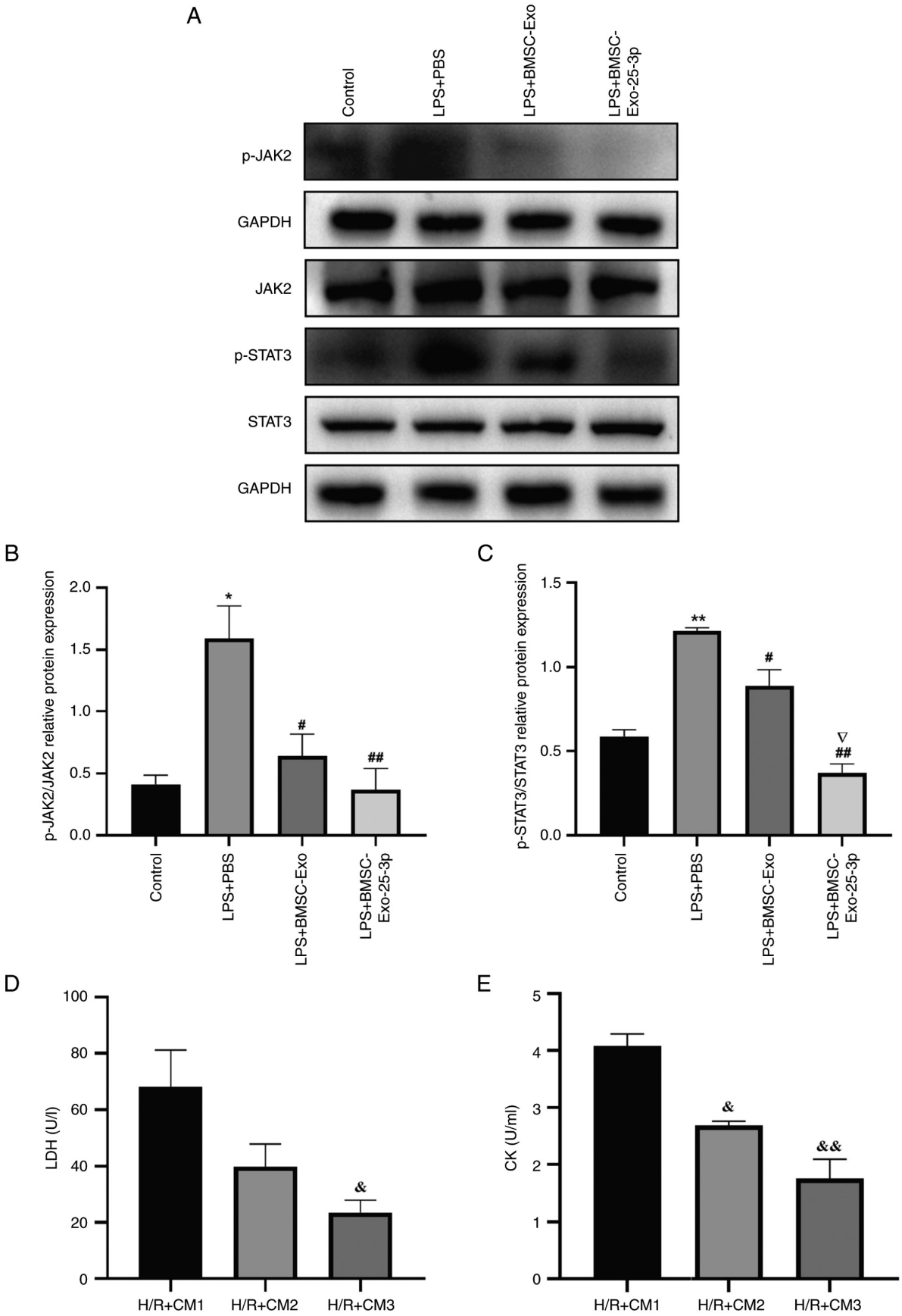

Figure 6. LPS-stimulated RAW 264.7 macrophage cocultured with H/R-induced H9C2 cells. (A) Representative western blotting images of the JAK2/STAT3 signaling pathway in LPS-stimulated RAW 264.7 cells. Quantitative analysis of (B) p-JAK2 and (C) p-STAT3. (D) LDH and (E) CK activity in cell culture supernatant of H9C2 cells pretreated with CM obtained from LPS-stimulated RAW 264.7 macrophages. **P<0.01, *P<0.05 vs. Control group. $^{\#\#}$P<0.01, $^{\#}$P<0.05 vs. LPS + PBS group. $^{\triangledown}$P<0.05 vs LPS + BMSC-Exo group. $^{\&\&}$P<0.01, $^{\&}$P<0.05 vs. H/R + CM1 group. All data were presented as mean ± SD. Exo, exosome; BMSC, bone marrow mesenchymal stem cells; LPS, lipopolysaccharide; JAK2, Janus kinase 2; p-, phosphorylated; STAT3, signal transducer and activator of transcription 3; LDH, lactate dehydrogenase; CK, creatine kinase; CM, conditioned medium.

results showed that the JAK2/STAT3 signaling pathway was activated in LPS-stimulated RAW 264.7 macrophages, as shown by the significant increase in the phosphorylation of JAK2 and STAT3. However, BMSC-Exo-25-3p inhibited the activation of this signaling pathway and significantly reduced the phosphorylation of JAK2 and STAT3 (Fig. 6A-C).

LPS-stimulated RAW 264.7 macrophage coculture with H/R-induced H9C2 cells. H9C2 cells were treated with CM obtained from LPS-stimulated RAW 264.7 macrophages as aforementioned to explore the role of the macrophage phenotype in H/R-induced H9C2 cell injury, and H9C2 cell culture supernatant was collected to analyze the enzymatic activity of LDH and CK. Compared with the PBS group, CM derived from BMSC-Exo-25-3p pre-intervention of RAW 264.7 macrophages significantly decreased the activities of LDH and CK in H/R-induced H9C2 cells (Fig. 6D and E).

Discussion

MIRI occurs after the ischemic myocardium restoring blood supply, and morbidity rates associated with MIRI have steadily increased since 2004 (53). Previous studies have shown that BMSCs promote wound healing and tissue repair by regulating the immune response and inhibiting inflammation and apoptosis (54,55). Several recent studies have indicated that BMSC-Exo could alleviate MIRI by inhibiting the expression of inflammatory factors or inflammatory mediators in the earlier inflammatory phase or the healing phase (56,57). miRNAs are considered important components of exosomes and largely determine their effects on receptor cells (58). Extensive research has confirmed that exosomes play a crucial role in intercellular communication by transporting miRNAs and proteins and have been found to reduce I/R-induced damage (53,59,60). Studies have reported that miR-25-3p in BMSC-Exo ameliorates liver I/R injury through PTEN (61,62). Exosomal miR-25-3p derived from MSCs has been shown to alleviate myocardial infarction by targeting proapoptotic proteins and enhancer of zeste homolog 2 (48). Although previous studies have shown that delivering miR-25-3p through stem cell extracellular vesicles can improve cardiac function and inhibit MIRI, the specific mechanism remains to be determined.

The present study explored the mechanism of miR-25-3p overexpression in BMSC-Exo in MIRI. An *in vivo* MIRI model in rats was estabilshed by ligating the anterior descending left coronary artery and an *in vitro* H/R model in H9C2 cells. BMSC-Exo carrying miR-25-3p protected against MIRI, as demonstrated by the finding that BMSC-Exo-25-3p reduced the incidence of arrhythmia and the myocardial infarction area in rats. Cardiac enzymes such as LDH and CK are released after myocardial injury (63) and are often used as markers of myocardial damage. Furthermore, the present study revealed a significant decrease in cardiac enzymatic activity following the overexpression of miR-25-3p.

After the onset of I/R, various injury-related factors are released to induce an inflammatory cascade in the heart. The inflammatory response involves the infiltration of inflammatory cells, including lymphocytes, neutrophils and macrophages, leading to the accumulation of proinflammatory cytokines and, ultimately, severe cardiac dysfunction (64). Inflammatory cell infiltration and the accumulation of proinflammatory cytokines can not only clear cell debris but also cause further damage and stress in surviving myocardial cells (65,66). Inflammatory monocytes enter the damaged surrounding area and transform into macrophages, which are the core mediators of cardiac inflammation and regulate tissue damage and repair (67). M1-like macrophages infiltrate damaged heart tissue, triggering the release of proinflammatory cytokines and local inflammatory responses. In contrast, M2-like macrophages have anti-inflammatory properties and are involved in tissue regeneration and remodeling (68,69), promoting wound healing and scar formation (49). In addition, promoting M2-type macrophage polarization has been shown to prevent I/R damage (49,70). BMSC-Exo plays an immunoprotective role in inflammatory reactions (71). The present study showed that the mRNA expression levels of IL-1 β and IL-6 increased after MIRI *in vivo*, and BMSC-Exo-25-3p reversed this effect. This finding suggested that BMSC-Exo, especially BMSC-Exo-25-3p, restricts M1-like macrophage polarization and promotes the polarization of M2-like macrophages after MIRI *in vivo*. The results were consistent with those reported in the literature (65).

Since the JAK/STAT signaling pathway is widely involved in the regulation of inflammation and immune responses, which play an important role in the progression of I/R (72), inhibiting JAK/STAT signaling pathway activation might alleviate inflammatory response and tissue damage in I/R (73,74). The results of the present study showed that BMSC-Exo-25-3p could decrease phosphorylated JAK2 and STAT3 in myocardial tissue, suggesting that BMSC-Exo-25-3p inhibited JAK2/STAT3 signaling pathway activation.

To verify that BMSC-Exo-25-3p regulates the polarization of macrophages concerning the JAK2/STAT3 signaling pathway, RAW264.7 macrophages were cultured *in vitro* and cocultured with H9C2 cells. After LPS stimulation, the mRNA expression levels of iNOS and IL-6 increased, suggesting that LPS induced M1-like macrophage polarization. BMSC-Exo, particularly BMSC-Exo-25-3p, reversed this effect, restricting M1-like macrophage polarization and promoting the polarization of M2-like macrophages after LPS stimulation. Similarly, the phosphorylation levels of the JAK2 and STAT3 proteins increased after LPS stimulation, while BMSC-Exo, particularly BMSC-Exo-25-3p, effectively reduced the phosphorylation of JAK2 and STAT3. Moreover, H9C2 cells were treated with CM obtained from LPS-stimulated RAW 264.7 macrophages to explore the role of the macrophage phenotype in H/R-induced H9C2 cell injury. The results showed that CM derived from BMSC-Exo-25-3p preintervention in RAW 264.7 macrophages significantly decreased the activities of LDH and CK in H/R-induced H9C2 cells. The present study demonstrated that BMSC-Exo, especially BMSC-Exo-25-3p, inhibited JAK2/STAT3 signaling pathway activation and induced the transformation of macrophages from the M1 to the M2 phenotype, reducing the inflammatory response and protecting against MIRI.

In addition to the indirect protective effects of BMSC-25-3p, whether BMSC-Exo-25-3p has a direct effect on H/R-induced H9C2 cells was investigated. Consistent with the literature, BMSC-Exo-25-3p uptake resulted in a significant increase in miR-25-3p in H9C2 cells and protected H9C2

cells from H/R-induced injury. Notably, it was also observed that BMSC-Exo-25-3p had a certain regulatory effect on the JAK2/STAT3 signaling pathway in H9C2 cells, which requires further investigation.

The present study has some limitations. First, the current understanding of macrophage polarization behavior is limited, and extensive research is required to fully comprehend the complexity of this process. Second, although BMSC-Exo-25-3p can regulate the polarization of macrophages through the JAK2/STAT3 signaling pathway, the direct mechanism of action of miRNA-25-3p remains to be further studied. Third, since promoting the polarization of M2-type macrophages is crucial for the cardioprotective effect of BMSC-Exo-25-3p, it is necessary to investigate how polarized macrophages protect the heart. Finally, although TTC-staining of myocardial tissue was performed to reflect myocardial injury, the present study was unable to assess the effects of miR-25-3p on heart injury *in situ*.

As a key medium of intercellular communication, and as a potential drug delivery system, exosomes will play an important therapeutic role in the future, especially in the area of heart repair, however at present, the clinical transformation of exosomes faces numerous problems and challenges. Currently, no exosome therapy has been approved for marketing, and methods of isolating exosomes with high purity, large quantities and a stable quality remain to be solved in the future.

In conclusion, in the present study, the protective mechanism of BMSC-Exo in MIRI was investigated. The results revealed that BMSC-Exo delivery of miR-25-3p caused a shift in the macrophage phenotype from the proinflammatory/M1 to the anti-inflammatory/M2 phenotype, reducing the inflammatory response and protecting against MIRI. The polarization of macrophages may be related to the JAK2/STAT3 signaling pathway. These findings provided a theoretical foundation for the use of BMSC-Exo as carriers of therapeutic drugs or genes in MIRI medical therapeutics, which may affect the prognosis of patients with coronary heart disease after thrombolysis or percutaneous coronary intervention.

Acknowledgments

Not applicable.

Funding

The present study was supported by The Luoyang City Social Development Public Welfare Project (grant no. 2302001A) and The Henan Province Scientific and Technology Research Project (grant no. 222103810051).

Availability of data and materials

The data generated in the present study may be requested from the corresponding author.

Authors' contributions

YD and JS developed the animal pathological models and cell models, and completed the molecular biological experiments. HS and CX assisted with the biochemical tests and *in vivo* imaging. YH was responsible for analyzing the data. SZ and SW assisted in the establishment of animal pathological models. JD designed the study and revised the manuscript. YD and JS confirm the authenticity of all the raw data. All authors read and approved the final version of the manuscript.

Ethics approval and consent to participate

All the experimental procedures were approved by The Animal Care and Ethics Committee of Henan University of Science and Technology (Luoyang, China; approval no. 2021-0392). and adhered to the guidelines for the care and use of laboratory animals outlined by the US National Institutes of Health.

Patient consent for publication

Not applicable.

Competing interests

The authors declare that they have no competing interests.

References

1. Gibbons RJ: Myocardial ischemia in the management of chronic coronary artery disease: Past and present. Circ Cardiovasc Imaging 14: e011615, 2021.
2. Safiri S, Karamzad N, Singh K, Carson-Chahhoud K, Adams C, Nejadghaderi SA, Almasi-Hashiani A, Sullman MJM, Mansournia MA, Bragazzi NL, *et al*: Burden of ischemic heart disease and its attributable risk factors in 204 countries and territories, 1990-2019. Eur J Prev Cardiol 29: 420-431, 2022.
3. Asaria P, Elliott P, Douglass M, Obermeyer Z, Soljak M, Majeed A and Ezzati M: Acute myocardial infarction hospital admissions and deaths in England: A national follow-back and follow-forward record-linkage study. Lancet Public Health 2: e191-e201, 2017.
4. Hausenloy DJ and Yellon DM: Myocardial ischemia-reperfusion injury: A neglected therapeutic target. J Clin Invest 123: 92-100, 2013.
5. Fan Q, Tao R, Zhang H, Xie H, Lu L, Wang T, Su M, Hu J, Zhang Q, Chen Q, *et al*: Dectin-1 contributes to myocardial ischemia/reperfusion injury by regulating macrophage polarization and neutrophil infiltration. Circulation 139: 663-678, 2019.
6. Liu R, Liu H, Yuan D, Chen Y, Tang X, Zhang C, Zhu P, Yang T, Zhang Y, Li H, *et al*: For patients with prior coronary artery bypass grafting and recurrent myocardial ischemia, percutaneous coronary intervention on bypass graft or native coronary artery?-A 5-year follow-up cohort study. Clin Cardiol 46: 680-688, 2023.
7. Chen Y, Du J, Zheng L, Wang Z, Zhang Z, Wu Z, Zhu X and Xiong JW: Chemical screening links disulfiram with cardiac protection after ischemic injury. Cell Regen 12: 25, 2023.
8. Miri R, Howlett SE and Knaus EE: Synthesis and calcium channel modulating effects of isopropyl 1,4-dihydro-2,6-dimethyl-3-nitro-4-(thienyl)-5-pyridinecarboxylates. Arch Pharm (Weinheim) 330: 290-294, 1997.
9. Li Z, Gao J, Sun D, Jiao Q, Ma J, Cui W, Lou Y, Xu F, Li S and Li H: LncRNA MEG3: Potential stock for precision treatment of cardiovascular diseases. Front Pharmacol 13: 1045501, 2022.
10. Algoet M, Janssens S, Himmelreich U, Gsell W, Pusovnik M, Van den Eynde J and Oosterlinck W: Myocardial ischemia-reperfusion injury and the influence of inflammation. Trends Cardiovasc Med 33: 357-366, 2023.
11. Hassanshahi A, Moradzad M, Ghalamkari S, Fadaei M, Cowin AJ and Hassanshahi M: Macrophage-mediated inflammation in skin wound healing. Cells 11: 2953, 2022.
12. Jia D, Chen S, Bai P, Luo C, Liu J, Sun A and Ge J: Cardiac resident macrophage-derived legumain improves cardiac repair by promoting clearance and degradation of apoptotic cardiomyocytes after myocardial infarction. Circulation 145: 1542-1556, 2022.

13. Xu M, Li X and Song L: Baicalin regulates macrophages polarization and alleviates myocardial ischaemia/reperfusion injury via inhibiting JAK/STAT pathway. Pharm Biol 58: 655-663, 2020.
14. Louiselle AE, Niemiec SM, Zgheib C and Liechty KW: Macrophage polarization and diabetic wound healing. Transl Res 236: 109-116, 2021.
15. Calle P and Hotter G: Macrophage phenotype and fibrosis in diabetic nephropathy. Int J Mol Sci 21: 2806, 2020.
16. Fu B, Xiong Y, Sha Z, Xue W, Xu B, Tan S, Guo D, Lin F, Wang L, Ji J, *et al*: SEPTIN2 suppresses an IFN-γ-independent, proinflammatory macrophage activation pathway. Nat Commun 14: 7441, 2023.
17. Wan E, Yeap XY, Dehn S, Terry R, Novak M, Zhang S, Iwata S, Han X, Homma S, Drosatos K, *et al*: Enhanced efferocytosis of apoptotic cardiomyocytes through myeloid-epithelial-reproductive tyrosine kinase links acute inflammation resolution to cardiac repair after infarction. Circ Res 113: 1004-1012, 2013.
18. Mahdiani S, Omidkhoda N, Rezaee R, Heidari S and Karimi G: Induction of JAK2/STAT3 pathway contributes to protective effects of different therapeutics against myocardial ischemia/reperfusion. Biomed Pharmacother 155: 113751, 2022.
19. Wu L, Tan JL, Wang ZH, Chen YX, Gao L, Liu JL, Shi YH, Endoh M and Yang HT: ROS generated during early reperfusion contribute to intermittent hypobaric hypoxia-afforded cardioprotection against postischemia-induced Ca(2+) overload and contractile dysfunction via the JAK2/STAT3 pathway. J Mol Cell Cardiol 81: 150-161, 2015.
20. Liao Y, Hu X, Guo X, Zhang B, Xu W and Jiang H: Promoting effects of IL-23 on myocardial ischemia and reperfusion are associated with increased expression of IL-17A and upregulation of the JAK2-STAT3 signaling pathway. Mol Med Rep 16: 9309-9316, 2017.
21. Yin Q, Zhao B, Zhu J, Fei Y, Shen W, Liang B, Zhu X and Li Y: JLX001 improves myocardial ischemia-reperfusion injury by activating Jak2-Stat3 pathway. Life Sci 257: 118083, 2020.
22. Sopjani M, Morina R, Uka V, Xuan NT and Dërmaku-Sopjani M: JAK2-mediated intracellular signaling. Curr Mol Med 21: 417-425, 2021.
23. Liu J and Jiang B: Sphk1 promotes ulcerative colitis via activating JAK2/STAT3 signaling pathway. Hum Cell 33: 57-66, 2020.
24. Shen Z, Huang W, Liu J, Tian J, Wang S and Rui K: Effects of mesenchymal stem cell-derived exosomes on autoimmune diseases. Front Immunol 12: 749192, 2021.
25. Yuan Y, Fan X, Guo Z, Zhou Z and Gao W: Metformin protects against spinal cord injury and cell pyroptosis via AMPK/NLRP3 inflammasome pathway. Anal Cell Pathol (Amst) 2022: 3634908, 2022.
26. Harrell CR, Jovicic N, Djonov V, Arsenijevic N and Volarevic V: Mesenchymal stem cell-derived exosomes and other extracellular vesicles as new remedies in the therapy of inflammatory diseases. Cells 8: 1605, 2019.
27. Zhang SJ, Song XY, He M and Yu SB: Effect of TGF-β1/SDF-1/CXCR4 signal on BM-MSCs homing in rat heart of ischemia/perfusion injury. Eur Rev Med Pharmacol Sci 20: 899-905, 2016.
28. Hatzistergos KE, Quevedo H, Oskouei BN, Hu Q, Feigenbaum GS, Margitich IS, Mazhari R, Boyle AJ, Zambrano JP, Rodriguez JE, *et al*: Bone marrow mesenchymal stem cells stimulate cardiac stem cell proliferation and differentiation. Circ Res 107: 913-922, 2010.
29. Davidson SM and Yellon DM: Exosomes and cardioprotection-A critical analysis. Mol Aspects Med 60: 104-114, 2018.
30. Lai RC, Arslan F, Lee MM, Sze NS, Choo A, Chen TS, Salto-Tellez M, Timmers L, Lee CN, El Oakley RM, *et al*: Exosome secreted by MSC reduces myocardial ischemia/reperfusion injury. Stem Cell Res 4: 214-222, 2010.
31. McDonald MK, Tian Y, Qureshi RA, Gormley M, Ertel A, Gao R, Aradillas Lopez E, Alexander GM, Sacan A, Fortina P and Ajit SK: Functional significance of macrophage-derived exosomes in inflammation and pain. Pain 155: 1527-1539, 2014.
32. Sun XH, Wang X, Zhang Y and Hui J: Exosomes of bone-marrow stromal cells inhibit cardiomyocyte apoptosis under ischemic and hypoxic conditions via miR-486-5p targeting the PTEN/PI3K/AKT signaling pathway. Thromb Res 177: 23-32, 2019.
33. Chen Q, Liu Y, Ding X, Li Q, Qiu F, Wang M, Shen Z, Zheng H and Fu G: Bone marrow mesenchymal stem cell-secreted exosomes carrying microRNA-125b protect against myocardial ischemia reperfusion injury via targeting SIRT7. Mol Cell Biochem 465: 103-114, 2020.
34. Cui H, He Y, Chen S, Zhang D, Yu Y and Fan C: Macrophage-derived miRNA-containing exosomes induce peritendinous fibrosis after tendon injury through the miR-21-5p/Smad7 pathway. Mol Ther Nucleic Acids 14: 114-130, 2019.
35. Xiong W, Qu Y, Chen H and Qian J: Insight into long noncoding RNA-miRNA-mRNA axes in myocardial ischemia-reperfusion injury: The implications for mechanism and therapy. Epigenomics 11: 1733-1748, 2019.
36. Zheng D, Li Z, Wei X, Liu R, Shen A, He D, Tang C and Wu Z: Role of miR-148a in mitigating hepatic ischemia-reperfusion injury by repressing the TLR4 signaling pathway via targeting CaMKIIα in vivo and in vitro. Cell Physiol Biochem 49: 2060-2072, 2018.
37. Wang X, Zhang X, Ren XP, Chen J, Liu H, Yang J, Medvedovic M, Hu Z and Fan GC: MicroRNA-494 targeting both proapoptotic and antiapoptotic proteins protects against ischemia/reperfusion-induced cardiac injury. Circulation 122: 1308-1318, 2010.
38. Wu JB, Ye XH, Xian SX and Dong MG: Expressions of SERCA2a and miR-25-3p/5p in myocardium of rats with heart failure and therapeutic effects of Xiefei Lishui recipe. Zhongguo Ying Yong Sheng Li Xue Za Zhi 33: 146-150, 2017 (In Chinese).
39. Wu D, Kang L, Tian J, Wu Y, Liu J, Li Z, Wu X, Huang Y, Gao B, Wang H, *et al*: Exosomes derived from bone mesenchymal stem cells with the stimulation of Fe_3O_4 nanoparticles and static magnetic field enhance wound healing through upregulated miR-21-5p. Int J Nanomedicine 15: 7979-7993, 2020.
40. Yang Z, Shi J, Xie J, Wang Y, Sun J, Liu T, Zhao Y, Zhao X, Wang X, Ma Y, *et al*: Large-scale generation of functional mRNA-encapsulating exosomes via cellular nanoporation. Nat Biomed Eng 4: 69-83, 2020.
41. Khan AA, Man F, Faruqu FN, Kim J, Al-Salemee F, Carrascal-Miniño A, Volpe A, Liam-Or R, Simpson P, Fruhwirth GO, *et al*: PET imaging of small extracellular vesicles via [^{89}Zr|Zr(oxinate)$_4$ direct radiolabeling. Bioconjug Chem 33: 473-485, 2022.
42. Kim CJ, Kuczler MD, Dong L, Kim J, Amend SR, Cho YK and Pienta KJ: Extracellular vesicle uptake assay via confocal microscope imaging analysis. J Vis Exp, 2022.
43. Chen G, Wang M, Ruan Z, Zhu L and Tang C: Mesenchymal stem cell-derived exosomal miR-143-3p suppresses myocardial ischemia-reperfusion injury by regulating autophagy. Life Sci 280: 119742, 2021.
44. Chen X, Li X, Zhang W, He J, Xu B, Lei B, Wang Z, Cates C, Rousselle T and Li J: Activation of AMPK inhibits inflammatory response during hypoxia and reoxygenation through modulating JNK-mediated NF-κB pathway. Metabolism 83: 256-270, 2018.
45. Du J, Li H, Song J, Wang T, Dong Y, Zhan A, Li Y and Liang G: AMPK activation alleviates myocardial ischemia-reperfusion injury by regulating Drp1-mediated mitochondrial dynamics. Front Pharmacol 13: 862204, 2022.
46. Lee SM, Son KN, Shah D, Ali M, Balasubramaniam A, Shukla D and Aakalu VK: Histatin-1 attenuates LPS-induced inflammatory signaling in RAW264.7 macrophages. Int J Mol Sci 22: 7856, 2021.
47. Bush EW and van Rooij E: miR-25 in heart failure. Circ Res 115: 610-612, 2014.
48. Peng Y, Zhao JL, Peng ZY, Xu WF and Yu GL: Exosomal miR-25-3p from mesenchymal stem cells alleviates myocardial infarction by targeting pro-apoptotic proteins and EZH2. Cell Death Dis 11: 317, 2020.
49. Yunna C, Mengru H, Lei W and Weidong C: Macrophage M1/M2 polarization. Eur J Pharmacol 877: 173090, 2020.
50. Cho DI, Kim MR, Jeong HY, Jeong HC, Jeong MH, Yoon SH, Kim YS and Ahn Y: Mesenchymal stem cells reciprocally regulate the M1/M2 balance in mouse bone marrow-derived macrophages. Exp Mol Med 46: e70, 2014.
51. Yu L, Zhang Y, Chen Q, He Y, Zhou H, Wan H and Yang J: Formononetin protects against inflammation associated with cerebral ischemia-reperfusion injury in rats by targeting the JAK2/STAT3 signaling pathway. Biomed Pharmacother 149: 112836, 2022.
52. Song M, Cui X, Zhang J, Li Y, Li J, Zang Y, Li Q, Yang Q, Chen Y, Cai W, *et al*: Shenlian extract attenuates myocardial ischaemia-reperfusion injury via inhibiting M1 macrophage polarization by silencing miR-155. Pharm Biol 60: 2011-2024, 2022.
53. Vicencio JM, Yellon DM, Sivaraman V, Das D, Boi-Doku C, Arjun S, Zheng Y, Riquelme JA, Kearney J, Sharma V, *et al*: Plasma exosomes protect the myocardium from ischemia-reperfusion injury. J Am Coll Cardiol 65: 1525-1536, 2015.

54. Fu X, Liu G, Halim A, Ju Y, Luo Q and Song AG: Mesenchymal stem cell migration and tissue repair. Cells 8: 784, 2019.
55. Yang Z, He C, He J, Chu J, Liu H and Deng X: Curcumin-mediated bone marrow mesenchymal stem cell sheets create a favorable immune microenvironment for adult full-thickness cutaneous wound healing. Stem Cell Res Ther 9: 21, 2018.
56. Zhao D, Bu Y, Shao H, Wang J, Li W and Li Q: Protective effect of exosomes derived from bone marrow mesenchymal stem cells on hypoxia reperfusion injury of cardiomyocytes. Cell Mol Biol (Noisy-le-grand) 70: 73-80, 2024.
57. Feng Y, Bao X, Zhao J, Kang L, Sun X and Xu B: MSC-derived exosomes mitigate myocardial ischemia/reperfusion injury by reducing neutrophil infiltration and the formation of neutrophil extracellular traps. Int J Nanomedicine 19: 2071-2090, 2024.
58. Wei Z, Qiao S, Zhao J, Liu Y, Li Q, Wei Z, Dai Q, Kang L and Xu B: miRNA-181a over-expression in mesenchymal stem cell-derived exosomes influenced inflammatory response after myocardial ischemia-reperfusion injury. Life Sci 232: 116632, 2019.
59. Davidson SM, Riquelme JA, Takov K, Vicencio JM, Boi-Doku C, Khoo V, Doreth C, Radenkovic D, Lavandero S and Yellon DM: Cardioprotection mediated by exosomes is impaired in the setting of type II diabetes but can be rescued by the use of non-diabetic exosomes in vitro. J Cell Mol Med 22: 141-151, 2018.
60. Chang D, Fan T, Gao S, Jin Y, Zhang M and Ono M: Application of mesenchymal stem cell sheet to treatment of ischemic heart disease. Stem Cell Res Ther 12: 384, 2021.
61. Li H, Lin W, Zhang G, Liu R, Qu M, Zhang J and Xing X: BMSC-exosomes miR-25-3p regulates the p53 signaling pathway through PTEN to inhibit cell apoptosis and ameliorate liver ischemia-reperfusion injury. Stem Cell Rev Rep 19: 2820-2836, 2023.
62. Kim MJ, Lim SG, Cho DH, Lee JY, Suk K and Lee WH: Regulation of inflammatory response by LINC00346 via miR-25-3p-mediated modulation of the PTEN/PI3K/AKT/NF-κB pathway. Biochem Biophys Res Commun 709: 149828, 2024.
63. Gao S, Li L, Li L, Ni J, Guo R, Mao J and Fan G: Effects of the combination of tanshinone IIA and puerarin on cardiac function and inflammatory response in myocardial ischemia mice. J Mol Cell Cardiol 137: 59-70, 2019.
64. Liu S, Chen J, Shi J, Zhou W, Wang L, Fang W, Zhong Y, Chen X, Chen Y, Sabri A and Liu S: M1-like macrophage-derived exosomes suppress angiogenesis and exacerbate cardiac dysfunction in a myocardial infarction microenvironment. Basic Res Cardiol 115: 22, 2020.
65. Lafuse WP, Wozniak DJ and Rajaram MVS: Role of cardiac macrophages on cardiac inflammation, fibrosis and tissue repair. Cells 10: 51, 2020.
66. Mack M: Inflammation and fibrosis. Matrix Biol 68-69: 106-121, 2018.
67. Wynn TA and Vannella KM: Macrophages in tissue repair, regeneration, and fibrosis. Immunity 44: 450-462, 2016.
68. Alvarez-Argote S and O'Meara CC: The evolving roles of cardiac macrophages in homeostasis, regeneration, and repair. Int J Mol Sci 22: 7923, 2021.
69. Choi JW, Kwon MJ, Kim IH, Kim YM, Lee MK and Nam TJ: Pyropia yezoensis glycoprotein promotes the M1 to M2 macrophage phenotypic switch via the STAT3 and STAT6 transcription factors. Int J Mol Med 38: 666-674, 2016.
70. Alam S, Liu Q, Liu S, Liu Y, Zhang Y, Yang X, Liu G, Fan K and Ma J: Up-regulated cathepsin C induces macrophage M1 polarization through FAK-triggered p38 MAPK/NF-κB pathway. Exp Cell Res 382: 111472, 2019.
71. Zhai Q, Chen X, Fei D, Guo X, He X, Zhao W, Shi S, Gooding JJ, Jin F, Jin Y and Li B: Nanorepairers rescue inflammation-induced mitochondrial dysfunction in mesenchymal stem cells. Adv Sci (Weinh) 9: e2103839, 2022.
72. Mascareno E, El-Shafei M, Maulik N, Sato M, Guo Y, Das DK and Siddiqui MA: JAK/STAT signaling is associated with cardiac dysfunction during ischemia and reperfusion. Circulation 104: 325-329, 2001.
73. Zhang WY, Zhang QL and Xu MJ: Effects of propofol on myocardial ischemia reperfusion injury through inhibiting the JAK/STAT pathway. Eur Rev Med Pharmacol Sci 23: 6339-6345, 2019.
74. Chen Y, Wu J, Zhu J, Yang G, Tian J, Zhao Y and Wang Y: Artesunate provides neuroprotection against cerebral ischemia-reperfusion injury via the TLR-4/NF-κB pathway in rats. Biol Pharm Bull 44: 350-356, 2021.